THE JOURNAL OF PHYSICAL CHEMISTRY C
A JOURNAL OF THE AMERICAN CHEMICAL SOCIETY

pubs.acs.org/JPCC

Article

Growth and Equilibrium Morphology of Hydrohalite ($NaCl{\cdot}2H_2O$) and Its Epitaxy with Hexagonal Ice Crystals

Dino Aquilano, Marco Bruno,* Linda Pastero, and Stefano Ghignone

Cite This: *J. Phys. Chem. C* 2021, 125, 6923–6932

Read Online

ACCESS | Metrics & More | Article Recommendations | Supporting Information

ABSTRACT: The experimental growth morphology of $NaCl{\cdot}2H_2O$, mineral hydrohalite (HH), is compared with that calculated at equilibrium, at 0 K. The HH surface structure is theoretically investigated through the Hartman–Perdok method: the growth characters of the different {*hkl*} forms are determined along with their possible surface profiles in order to calculate, at the DFT level, their specific surface energies in the presence of vacuum. The striking difference between the calculated equilibrium shape (ES) and the observed growth shape (GS) is interpreted on the ground of a privileged epi-adsorption of {00.1}, the most important form of hexagonal ice (I_h) on the observed dominant {010} form of HH. The sharp pseudo-hexagonality of the {010} HH-form (substrate) seems to be the keystone to understand the very good epitaxy with the {00.1} pinacoid (deposit) of Ice (I_h).

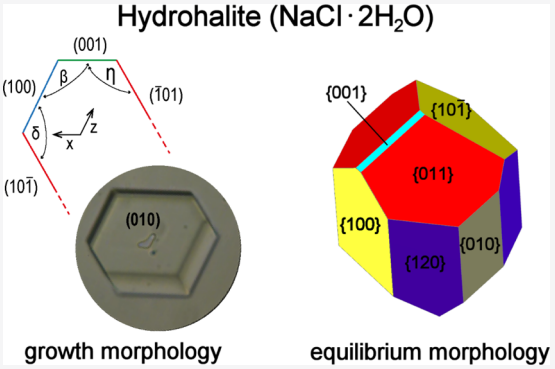

1. INTRODUCTION

$NaCl{\cdot}2H_2O$, the mineral hydrohalite (HH), is the only compound formed in the $NaCl–H_2O$ system; it melts under its own vapor pressure at −0.1 °C, converting to halite (NaCl).[1] Historically, large HH single crystals were grown by Mitscherlich,[2] who made the first crystallographic study of this compound and the related di-hydrates of NaBr and NaI.

HH is described as very rare and is one of a group of minerals we might dub "musherals" because they are 50% or more water. Like many other minerals, it requires extremely restricted physical or chemical conditions to form. It is significant for three reasons. First, whenever a mixture of NaCl and brine freezes, much of the brine freezes to make HH. Thus, it is rare in the sense we do not often see concentrated brine freeze, but where it does happen, like in Antarctica, HH is common. Second, strictly speaking, HH does not melt. It breaks down at 0 °C to brine and NaCl (halite) or "sweats" out the water. Thus, it is possibly the easiest example of incongruent melting to understand. Third, while conditions for the HH formation might be uncommon on Earth, they are probably very common on Mars and the interiors of icy satellites.[3−6]

A new mechanism for ice formation in the troposphere has been recently proposed by Wise et al.[7] Through lab-experiments, they showed the crystallization of a NaCl hydrate upon efflorescence of small NaCl droplets at low temperatures, "... this hydrate being a better ice nucleus than dry NaCl particles, as it does not require any significant supersaturation at temperature below about 235 K". More recently, Wagner and Möhler[8] provided additional evidence that crystalline HH particles are able to act as substrates for heterogeneous ice nucleation in the deposition mode.

In all the quoted works, careful observations and rigorous experiments were described, concerning the role exerted by both NaCl and HH on the heterogeneous nucleation of icy particles. Both thermodynamics and nucleation kinetics have been used to interpret the experimental results in the light of the sole "chemical" point of view. In other words, solid particles such as NaCl, H_2O, and $NaCl{\cdot}2H_2O$, were treated as bulk-crystals, like they do not have faces. Consequently, the mutual interplay among the three phases involved in a complex "crystal growth through interactions among crystal surfaces" has never been considered till now. Furthermore, it is well known how a crystalline substrate could influence the deposition and the structure of the first layers of ice.[9,10]

Aiming to bridge this gap, we shall determine the theoretical epitaxial compatibility between the HH crystal surfaces and those of the hexagonal polymorph (I_h) of the ice crystal, in order to quantitatively explain the heterogeneous nucleation of Ice, favored by HH crystal surfaces working as the substrate. To do this, we did the following:

(i) The HH bulk structure was investigated in the light of the periodic bond chain (PBC) theory (i.e., Hartman–Perdok method),[11−13] in order to find the characters of

Received: January 20, 2021
Revised: March 6, 2021
Published: March 18, 2021

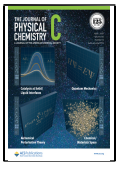

https://doi.org/10.1021/acs.jpcc.1c00527
J. Phys. Chem. C 2021, 125, 6923–6932

its crystallographic {*hkl*} forms: flat (F), stepped (S), or kinked (K).

(ii) The specific surface energy values (γ_{hkl}), at 0 K, was evaluated for both all F- and the low-index S-forms, in order to draw the athermal equilibrium shape (ES) of the crystal.

(iii) A ranking was also carried out concerning the lattice coincidences between {00.1}-Ice (I_h) and suitable HH crystal surfaces in order to find their possible epitaxies. The reason why the {00.1}-pinacoid of Ice has been chosen is strictly related to the hexagonality of its 2D lattice which could be ideally coupled with the HH pseudo-hexagonality.

2. EXPERIMENTAL SECTION

Crystallization of HH was followed in situ using an Olympus BX60 polarized light microscope (4×, 10×, 50×, 100× long focal distance objectives) equipped with a JVC KY-F55B 3 color digital camera—CCD and a Linkam cryo-thermostatic plate THMS600 (−196 to +600° C).

A solution of saturated NaCl at equilibrium with the solid sodium chloride was prepared at room temperature.

A droplet of RT-saturated NaCl solution was placed between two glass slides (5 mm diameter and 100 μm thick) to avoid halite precipitation at the solution/air interface that will affect HH nucleation and growth. By doing in this way, the double glass slide becomes a crystallization micro-vessel spontaneously sealed at the edges by the precipitation of halite by evaporation of the solvent. The crystallizing system then becomes closed − no solvent loss by evaporation from the micro-vessel is allowed. The supersaturation is regulated by thermal control. The crystallization micro-vessel is placed on the Linkam cryo-thermostatic plate and undergoes thermal cycles with a maximum range of −30/−5/−30 °C and gradients of 10, 15, and 20 °C/min, according to the binary phase diagram for the system H_2O−NaCl reported in the literature.[14] The solution is metastable, and thus no nucleation is reached without recurring to a trigger. The nucleation was triggered by quenching the solution at −60 °C and then resumed the normal thermal cycle. According to Ostwald's ripening, thermal cycles make it possible to reduce the number of nuclei and increase their size to render the growth morphology better (Figure 1).

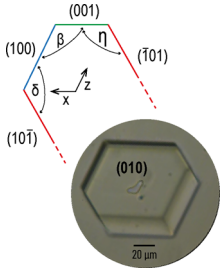

Figure 1. HH crystal lying on its (010) pinacoidal form and showing its morphological pseudo-hexagonality. Angles: β = 114.41°, η = 121.60°, and δ = 123.99°, between the faces: (100), (001), (10$\bar{1}$), that are coherent with respect to those of the structural cell, as described by Klewe and Pedersen.[15] Temperature −30 °C, thermal cycle −30/−5/−30 °C.

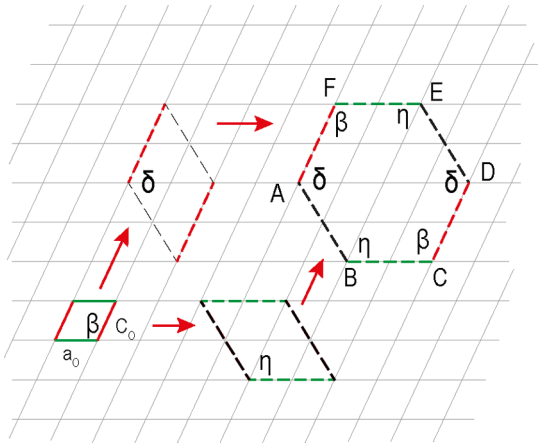

Figure 2. HH-[010] projection showing the 2D-lattice associated to the {010} form (parallel to the drawing plane). From the elementary 2D-cell (a_0, c_0, β), with multiplicity (1×), two kinds of equivalent supercells with multiplicity (4×) can be generated, along the six-sided pseudo-hexagonal cell with multiplicity (12×). Sides (in Å): AB = 13.9064, BC = 12.6626, and CD = 13.0058. Angle: β = 114.407°, δ = 123.974°, and η = 121.619°.

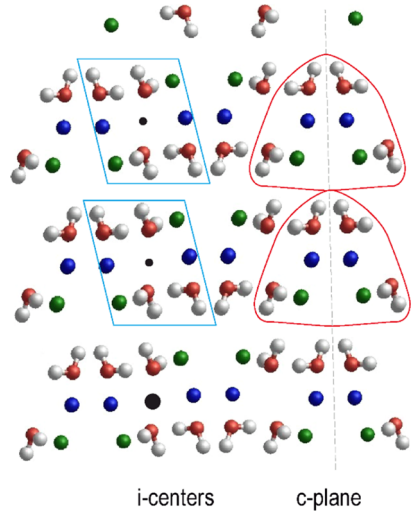

Figure 3. Two alternative structures of the PBC [001], viewed along the [001] direction. The structure of the PBC $[001]_A$ (right side) is mirror-symmetric, while the structure of the PBC $[001]_B$ (left side) is center-symmetric. Both the PBCs show polarity along the directions [001] and [100], while the polarity is canceled out along the [010] direction owing to both the inversion centers and the symmetry glide plane *c*// 010. Na (blue); Cl (green); O_{water} (red); H_{water} (grey).

3. RESULTS AND DISCUSSION

HH is a monoclinic crystal, the cell parameters (in Å) being a_0 = 6.331, b_0 = 10.118, c_0 = 6.503; $\alpha = \gamma = 90$, β = 114.41°.[15] Its space group is: $P2_1/c$ (S.G. no. 14), with the extinction rules

$$h0l \rightarrow l = 2n;\ \ 0k0 \rightarrow k = 2n;\ \ 00l \rightarrow l = 2n;\ \ hkl \rightarrow k + l = 2n$$

Prior consideration is required about the HH bulk structure. In spite of its monoclinic symmetry, HH exhibits a marked pseudo-hexagonality (Figure 1). In fact, a 2D-supercell in the lattice plane 010 can be found, as shown in Figure 2. Its symmetry is due to the diad axis A_2//[010], the sides (in Å) being the three vectors: 2×[001] = 13.006, 2×[100] = 12.663,

https://doi.org/10.1021/acs.jpcc.1c00527
J. Phys. Chem. C 2021, 125, 6923−6932

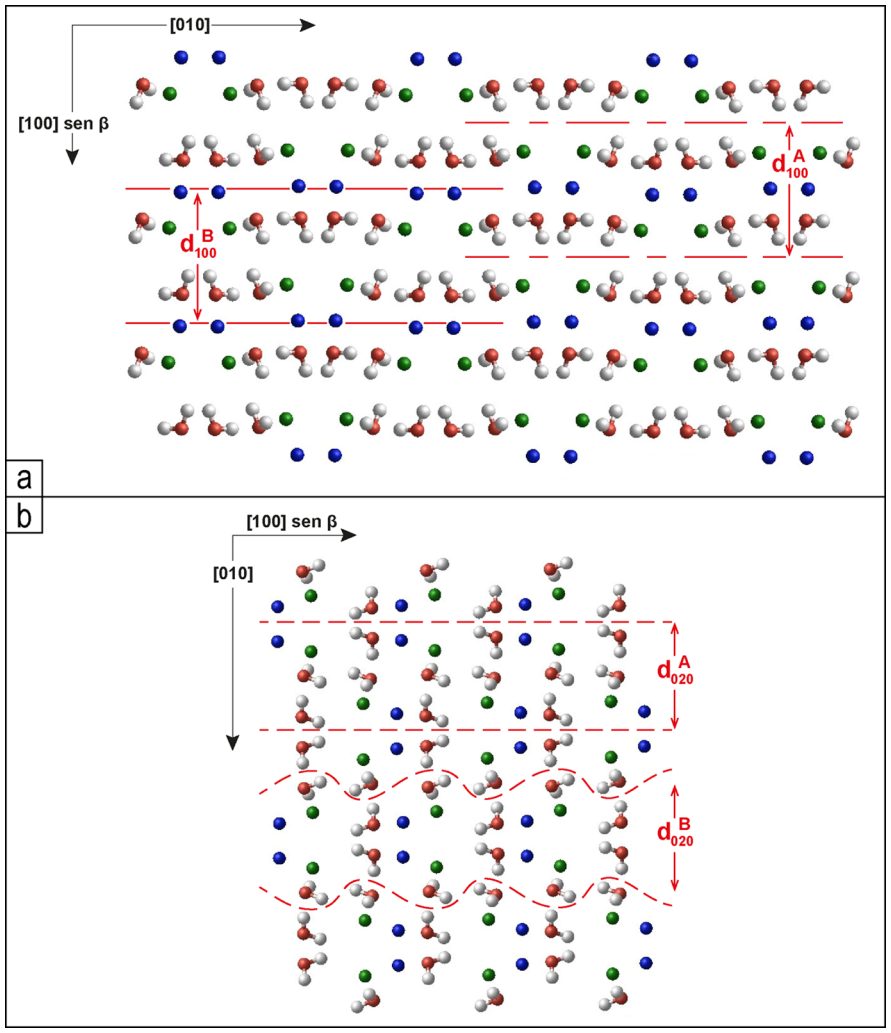

Figure 4. HH structure viewed along the [001] direction. (a) Slices of thickness d_{100} are represented, along with the surface profiles of the $\{100\}_A$ and $\{100\}_B$ flat (F) pinacoid. (b) Slices of the allowed thickness d_{020} are represented, along with their flat surface profiles, $\{010\}_A$ and $\{010\}_B$.

and 2×[101] = 13.906. Their mean value being 13.192 Å, the dispersion of the side lengths ranges between −4.01 and +5.42%. Moreover, the internal angles of the supercell are $\beta = 114.407°$, $\eta = 121.619°$, $\delta = 123.974$, their angular deviation ranging between −5.59 and +3.97% with respect to that of the perfect hexagonality. Hence, both linear and angular misfits play in favor of a good pseudo-hexagonality. This searching is not weird, if one looks at the ability of HH particles to favor the heterogeneous nucleation of the hexagonal polymorph of ice.[7,8] Accordingly, we will try to find the lattice compatibility, if any, between the HH-{010} form and the {00.1} one of the hexagonal polymorphic phase of Ice (I_h).

3.1. HH Theoretical Morphology, Viewed through the PBC Analysis on Its Bulk Structure. *3.1.1. [001] Zone: the Pinacoids {100} and {010} and the Prisms {110}, {120}, {140}, and {180}.* The most important sequence of uninterrupted strong bonds between first neighbors develops along the [001] direction. We are dealing with a helicoidal −Na−Cl− chain having the repeat period $c_0 = 6.5029$ Å. With reference to the set of atomic coordinates listed in Table S1 (Supporting Information), the structure of the [001] chain reads as follows: Cl_1−Na_1−Cl_4−Na_4−Cl_1 [001], where the couple (Cl_4−Na_4) is related to the couple (Cl_1−Na_1) by the glide mirror *c*, parallel to 010, of the space group $P2_1/c$ (Figure 3, right side). Four water molecules are needed to fulfil the stoichiometry of the PBC $[001]_A$; the easiest way is to choose those realizing the following bonds: Na_1−W_{24}, Na_1−W_{14} $[\bar{1}00]$, Na_4−W_{11} $[\bar{1}00]$, and Na_4−W_{21} [001], as drawn in Figure 3. Two Cl···H−O_{water} hydrogen bonds complete the PBC $[001]_A$, namely, Cl_1−W_{24} and Cl_4−W_{21}, which are also related each other by the *c* plane. There is another way to choose a [001] PBC: as drawn in Figure 3 (left side), the islands contain the PBC $[001]_B$, which are center-symmetric. The duplicity of the PBC $[001]_{A,B}$ entails that some surface profiles of the forms {*hk*0}, that belong to the [001] zone, will not be unique.

The screw diad axis 2_1//[010] reproduces the [001] PBCs within the unit cell; thus, one can search for other PBCs within the slices of thickness d_{hk0} allowed by the extinction rules, in order to find the growth character of the forms {*hk*0}, that could fulfil the requirements of the Hartman−Perdok morphological method.

The screw diad axis 2_1//[010] reproduces the [001] PBCs within the unit cell; at first sight, two important flat (F) forms can be found in the [001] zone: the pinacoids {100} and {010}.

The [010] PBC is formed through the four bonds developing between two consecutive PBCs along the *y* axis: Na_2 $[\bar{1}00]$−W_{23} $[\bar{1}00]$, Na_2 $[\bar{1}00]$−W_{21} [001], and Cl_4−W_{13} and Cl_2−W_{23}. Thus, the two PBCs, [001] and [010], run within a center-

https://doi.org/10.1021/acs.jpcc.1c00527
J. Phys. Chem. C 2021, 125, 6923−6932

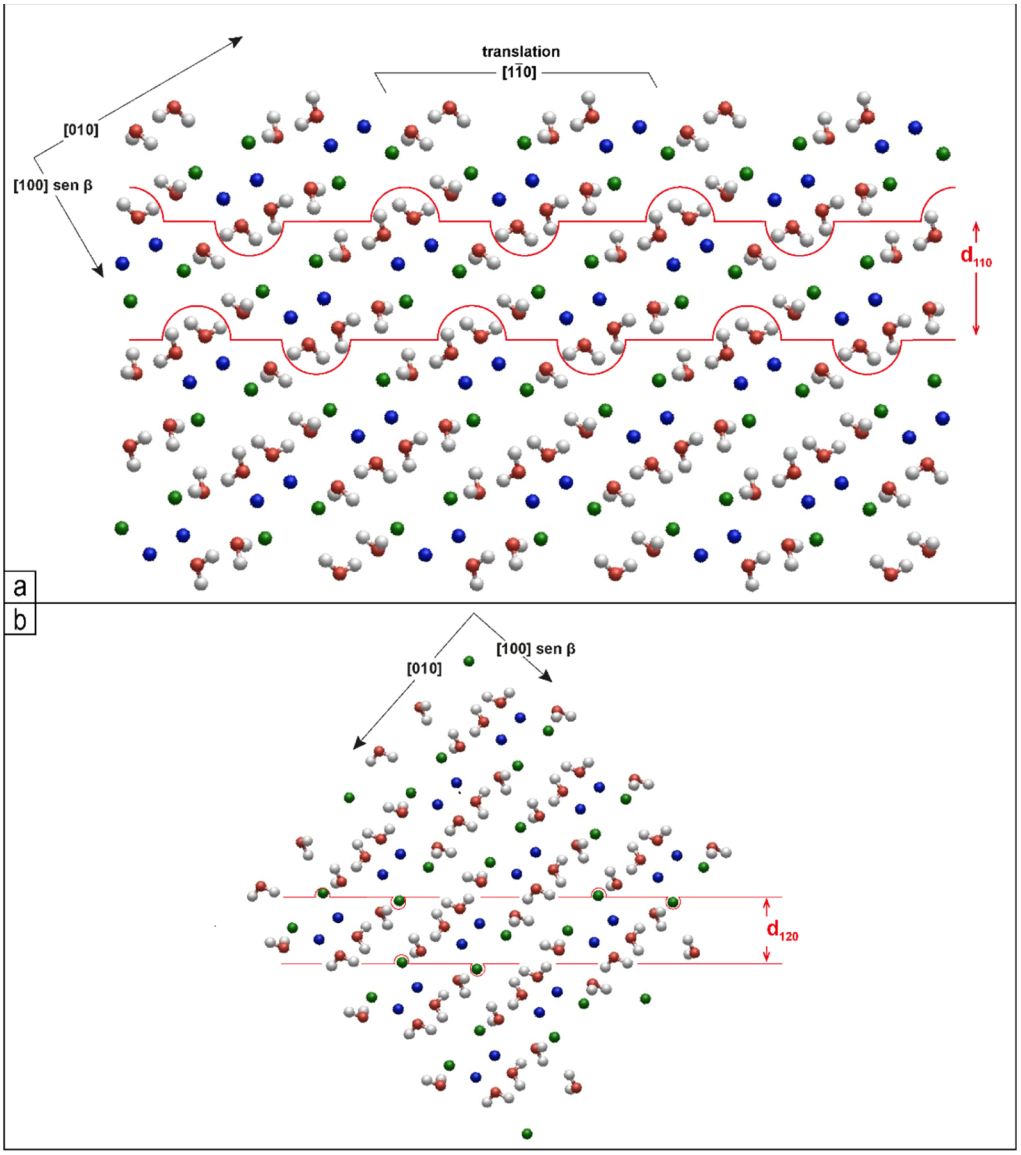

Figure 5. HH structure viewed along the [001] direction. (a) Center-symmetric slice of thickness d_{110} is represented, along with the surface profile of the prismatic {110} form. Only the slice d_{220} is allowed by the extinction rules, and then, the prism {110} is a stepped form. It is built by the PBCs [001] which are bound by the longest and weak Cl···H hydrogen bonds, along the [1$\bar{1}$0] direction, within the slice of thickness d_{110}. Direction [010] is parallel to the Na^+ rows (as in Figure 4a). (b) Center-symmetric slice of thickness d_{120} is represented along with the surface profile of the {120}-F prismatic form. It is built by the PBCs [001] which are bound by the longest and weak Cl···H bonds, along the [2$\bar{1}$0] direction (horizontal in Figure 5b).

symmetric slice of thickness d_{100}, which is allowed by the extinction rules.

The pinacoid {100} shows two alternative surface profiles. In the first one, the center-symmetric $\{100\}_A$, all Na^+ ions are located midway in the d^A_{100} slice, while both Cl^- ions and water molecules lie on the outmost layers of the slice. Further, adjacent d^A_{100} slices are separated by ideal planes containing neither ions nor molecules, but only an ideal 2D lattice built by symmetry centers only. Hence, such a slice profile need not be reconstructed. In the second one, $\{100\}_B$, all Na^+ ions are located in the outmost layer of the slice and are shared by adjacent d^B_{100} slices; accordingly, this surface profile has to be reconstructed, one-half of Na^+ ions belonging to one slice and the other half to the adjacent one. This proves that {100} has character F and that its most stable surface profile should be that where only the hydrogen bonds are interrupted between two adjacent d_{100} slices (Figure 4a). These are likely the reasons why the plane 100 represents the HH easy cleavage[16,17] and the pinacoid {100} should appear, at least qualitatively, as the most stable form of the crystal.

The pinacoid {010}. Within a slice of thickness d_{020}, which fulfils the constraint $0l0 = 2n$, the [100] PBC develops, linking two adjacent [001] PBCs through the already mentioned weak hydrogen bonds. Hence, the {010} form also has F character. Two adjacent d_{020} slices are joined by two Na−W bonds (namely, Na_2 [$\bar{1}$00]−W_{23} [$\bar{1}$00] and Na_2 [$\bar{1}$00]−W_{21} [001]) and two Cl−W hydrogen bonds (Cl_4−W_{13} and Cl_2−W_{23}); the two {010} stable surface profiles are represented in Figure 4b. The slice d^A_{010} is center-symmetric and made by the PBCs $[001]_B$, while the wavy slice d^B_{010} is mirror-symmetric and made by the PBCs $[001]_A$.

3.1.1.1. Two prisms can be found within the [001] zone: {110} and {120}. The prism {110}. Let us consider two adjacent PBCs $[001]_A$, symmetry related by the inversion centers, as

https://doi.org/10.1021/acs.jpcc.1c00527
J. Phys. Chem. C 2021, 125, 6923−6932

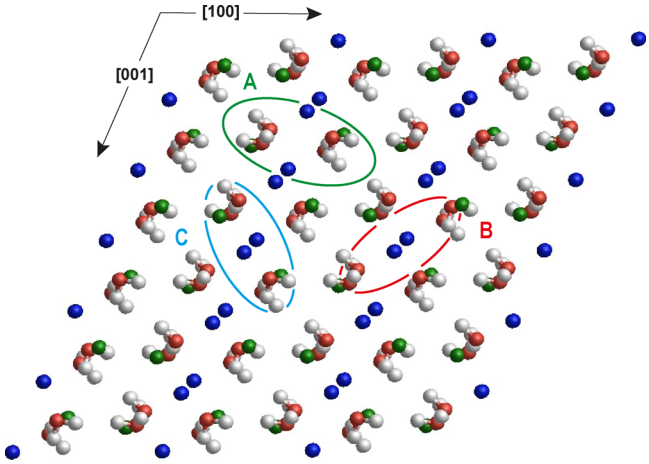

Figure 6. Structure of the PBCs $[010]_{A,B,C}$. The position and the multiplicity of Na^+ ions (blue) indicate that each elementary cell contains two PBCs.

represented in Figure 5a. They are connected by Cl−H_{water} bonds by the weak PBC $[1\bar{1}0]$, within a slice of thickness d_{110}. Consequently, the slice d_{110} is center-symmetric, but the F character of the form {110} is not allowed since the extinction rules are not fulfilled in this case, the constraints requiring the thickness d_{220}. This is the reason why the form {110} has stepped (S) character; nevertheless, we will consider it when calculating the specific surface energy values of the HH crystal surfaces, in order to foresee its equilibrium form. The {110} prism has a unique surface profile, because no other d_{110} slice can be generated through the PBC $[001]_B$.

The prism {120}. The slice of thickness d_{120} contains [001] chains built-up by mirror symmetric NaCl·H_2O units, stoichiometrically completed by adding two water molecules. These chains are connected within the d_{120} slice, through the inversion centers, by the longest and weak Cl···H bonds, along the $[2\bar{1}0]$ direction. The slice thickness fulfills the extinction rule: $hkl \rightarrow k + l = 2n$, and then, the prism {120} has F character (Figure 5b).

From a more detailed analysis, it comes out that two other prisms, {140} and {180}, can be found in the [001] zone, the corresponding slices, d_{140} and d_{180}, fulfilling the constraints of the extinction rules. Nevertheless, we will not consider them in the study, since it is easy foreseeing their low morphological importance; as a matter of fact, none of the [001] PBCs can be contained within these slices, because the lateral dimension of the [001] PBC is too large with respect to their thickness. Accordingly, they cannot be considered as F forms; hence, their slice energy will be weak, which implies high surface energy values. Thus, it is unlikely that they shall appear both in the equilibrium and growth morphology.

3.1.2. [010] Zone: the Pinacoids {001}, {10$\bar{1}$}, {102}, {10$\bar{2}$}, and {100}. As represented in Figure 6, three kinds of PBCs run along the unique symmetry axis, $A2_1//[010]$. They are identified as the PBC $[010]_A$, symmetrically centered around the diad axis, and the PBCs $[010]_{B,C}$, both center-symmetric.

The pinacoid {001}. According to whether one chooses the PBC $[010]_A$ or $[010]_B$, two different {001} surface profiles can be obtained. Remembering that the growth layers of these forms could have the thickness d_{002}, owing to the extinction rule: $00l \rightarrow l = 2n$, the surface profile $\{001\}_A$ will be terminated by Na^+ ions, while the surface profile $\{001\}_B$ will be exposed to the mother phase of both Cl^- ions and water molecules (Figure 7a). This pinacoid has F character.

Other pinacoids: {10$\bar{2}$}, {102}, {10$\bar{1}$}, and {100} are found, in the zone with the [010] axis (Figure 7b):

(i) {10$\bar{2}$}, generated by the PBC $[010]_A$ and associated with the slice of thickness $d_{10\bar{2}}$, which shows the Na^+ ions on the outmost layer of the slice. Within this slice, allowed by the extinction rule $h0l \rightarrow l = 2n$, a second PBC runs, which is made by the bonds developing along the direction [201]. Hence, the form {10$\bar{2}$} has F character;

(ii) {102}, generated by the PBC $[010]_B$ and associated with the slice of thickness d_{102}, which shows the Na^+ ions in the middle of the slice. This slice is allowed as well by the extinction rule and contains another PBC running along the direction $[\bar{2}01]$. Hence, {102} has F character.

(iii) {10$\bar{1}$}, generated by the PBC $[010]_C$, can grow by layers of thickness $d_{20\bar{2}}$ (fulfilling the constraint $h0l \rightarrow l = 2n$), that is, one-half of the not allowed slice of thickness $d_{10\bar{1}}$. Its character is also F, due to the existence of another PBC in the slice, namely, the chain running along the direction [101].

(iv) {100}, that can show two alternative surface profiles, both related to a slice with thickness d_{100}, fulfilling the extinction rules: (a) the first one, related to a center-symmetric slice, has the Na^+ ions in the middle of the slice and can be generated from any of the PBCs $[010]_{A,B,C}$; (b) the second one, associated with a d_{100} slice having in the middle the screw axes [010], is surface-terminated by the Na^+ ions. {100} has F character, its profiles, $\{100\}_A$ and $\{100\}_B$, are represented in Figure 7c. This result is coherent with that we already obtained (Figure 4a) when analyzing the zone [001].

3.1.3. [100] Zone: the Prism {011}. In Figure 8, the PBC [100] with its inner bonds is represented. It is center-symmetric, as the PBC $[001]_B$ and the PBCs $[010]_{B,C}$. Accordingly, it does not show polar character. The glide plane *c*, which is parallel to the form {010}, reproduces this PBC along the set of the symmetry-equivalent directions $\langle 01\bar{1} \rangle$, therefore giving rise to four d_{011} slices. This thickness fulfils the extinction rule: $k + l = 2n$, for the {*hkl*} forms and, consequently, the prism {011} has flat character. The d_{011} slices are center-symmetric, and their surface profile is unique.

The [100] zone also belongs to the forms {010} and {001} that have been already discussed in the Sections 3.1.1 and 3.1.2.

3.2. Surface Specific Energies of the Six Pinacoids: {100}, {010}, {001}, {10$\bar{1}$}, {102}, and {10$\bar{2}$}, and the Three Prisms: {011}, {110}, and {120}. The Corresponding Athermal ES (Wulff's Plot at 0 K) of the HH Crystal. The crystal surfaces were simulated by using the 2D periodic slab model[18] and the *ab initio* CRYSTAL14 code.[19−21] The calculations were performed at the DFT (density functional theory) level: the B3LYP Hamiltonian was adopted.[22−24] Further computational details (e.g., basis set and the thresholds controlling the accuracy of the calculations) are reported in the Supporting Information.

The CRYSTAL14 output files, listing the optimized fractional coordinates and optimized 2D cell parameters of the (100), (010), (001), (10$\bar{1}$), (102), (10$\bar{2}$), (110), and (120) slabs, are freely available at http://mabruno.weebly.com/download. All of these slabs are charge neutral and preserve the inversion center or a mirror plane, to ensure that the dipole moment perpendicular to the slab is equal to zero.

The specific surface energy γ (erg/cm^2) at T = 0 K was calculated by means of the relation[18]

https://doi.org/10.1021/acs.jpcc.1c00527
J. Phys. Chem. C 2021, 125, 6923−6932

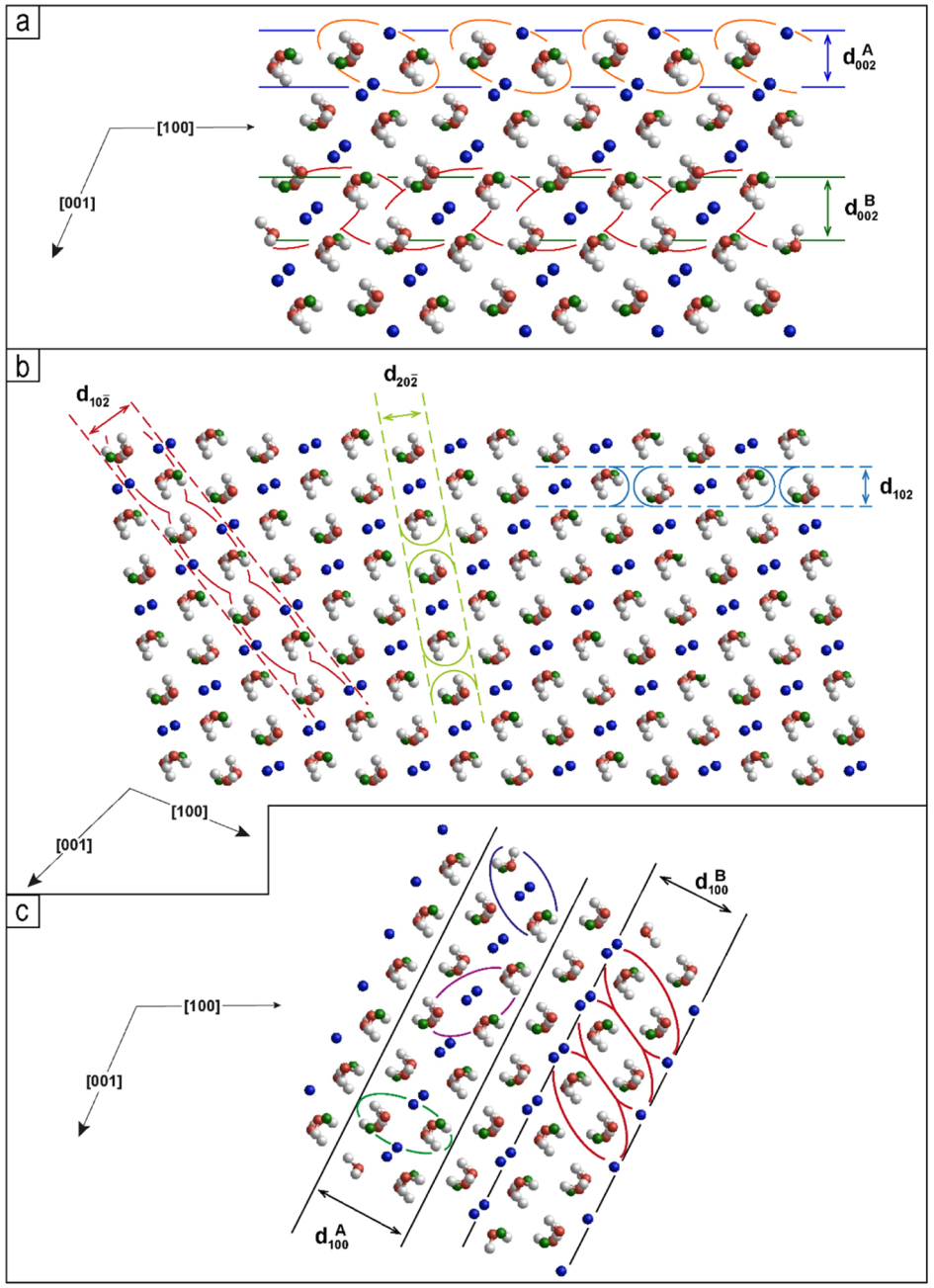

Figure 7. Projection along the [010] direction. (a) Surface profiles (A,B) of the form {001}, depending on the PBC $[010]_{A,B}$. In the first case (A), the symmetry of the slice is ruled by the $A2_1$ axes//[010] and the Na^+ ions terminate the slice; in the second case (B), the slice is center-symmetric and the Na^+ ions lie in the middle of the slice. In both cases, the slices do not show polarity orthogonally to the {001} profile, and hence, no surface reconstruction is required. (b) Surface profiles of the forms: $\{10\bar{2}\}$, {102}, and $\{10\bar{1}\}$, as obtained from the PBCs $[010]_A$, $[010]_B$, and $[010]_C$, respectively (see Figure 6). (c) Surface profiles $\{100\}_A$ and $\{100\}_B$ that belong to the pinacoid {100}.

$$\gamma = \lim_{n\to\infty} Es(n) = \lim_{n\to\infty} \frac{E(n)_{slab} - nE_{bulk}}{2A} \quad (1)$$

$$\frac{\gamma_1}{h_1} = \frac{\gamma_2}{h_2} = ... \frac{\gamma_3}{h_3} = ... = \text{constant} \quad (2)$$

where $E(n)$ and E_{bulk} are the energies of a n-layer slab and the bulk, respectively; A is the area of the primitive unit cell of the surface. $E_s(n)$ is thus the energy (per unit area) required for the formation of the surface from the bulk. When $n \to \infty$, $E_s(n)$ will converge to the surface energy per unit area (γ).

The specific surface energies are listed in Table 1, whereas the resulting ES is illustrated in Figure 9, as obtained by drawing the Wulff's plot according to the Gibbs–Wulff's theorem[25] where h_i represents the distance of the ith face from an ideal center (Wulff's point) of a convex polyhedron. It is worth noting that the surface profiles entering the ES are those that have the minimum surface energy values. As an example, for the (100) face, only the profile $(100)_A$ will be considered while, for the face (001), the surface profile $(001)_A$ will prevail on the alternative $(001)_B$.

When considering the γ values (Table1) coupled with the configuration of surface profiles (Figures 4–8), it follows that

https://doi.org/10.1021/acs.jpcc.1c00527
J. Phys. Chem. C 2021, 125, 6923–6932

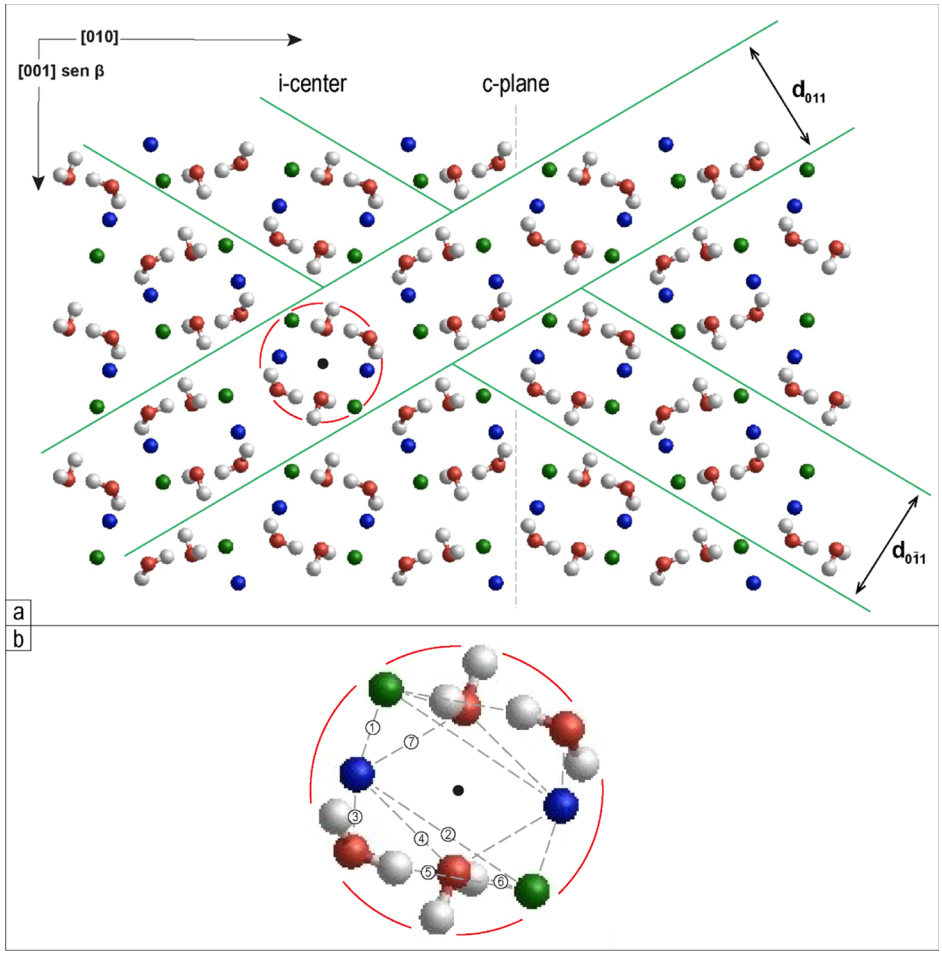

Figure 8. Projection along the [100] direction. (a) Center-symmetric [100] PBCs can be inscribed in ideal circles and are reproduced by the glide mirror planes $c//010$. Two slices are drawn, with thickness d_{011} and $d_{01\bar{1}}$, respectively, parallel to two out of the four faces building the prism {011}. (b) Inner bonds (in Å) of the [100] PBC are drawn: (1) = 2.792, (2) = 4.575, (3) = 2.458, (4) = 2.379, (5) = 2.440, (6) = 2.350, and (7) = 2.383.

Table 1. Ranking of HH Specific Surface Energies γ (erg/cm^2), Calculated, at 0 K and at Quantum-Mechanical Level[a]

form	γ (erg/cm^2)
$*\{100\}_A$	187
$*\{011\}$	210
$*\{120\}$	215
$*\{10\bar{1}\}$	217
$*\{010\}_A$	234
$*\{001\}_A$	237
$*\{010\}_B$	242
$\{110\}$	252
$\{102\}$	269
$\{10\bar{2}\}$	273
$\{001\}_B$	278
$\{100\}_B$	291

[a]Surface profiles marked with * enter the ES.

both position and orientation of electrical water dipoles with respect to the allowed slices is crucial to determine the γ_{hkl} value. The form {100} represents an extreme example. In the $\{100\}_A$ slice, Na^+ ions lie in the middle, while Cl^- ions and water molecules occupy the outmost layers limiting the slice; moreover, water dipoles point to the outside of the slice. On the contrary, in the $\{100\}_B$ slice, Na^+ ions are located in the outmost layers, while Cl^- and water occupy the middle of the

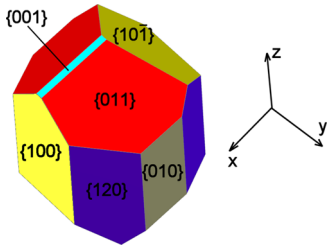

Figure 9. Theoretical HH ES, calculated at 0 K, with respect to the vacuum, is built by the pinacoids: {100}, {001}, {10$\bar{1}$}, and {010} and by the prisms: {120} and {011}. In spite of the sharp monoclinic symmetry of the crystal bulk, the theoretical ES is rather isotropic.

slice and water dipoles point inward. As a consequence, the γ value of $\{100\}_B$ is 55.6% higher than that of $\{100\}_A$. Moreover, it is worth outlining that $\gamma^A_{\{100\}} = 187$ erg/cm^2, that is, by far the lowest among the surface energy values, *quantitatively* proves that 100 represents the easy cleavage of the HH crystals.

The other forms in Table 1 also follow this trend as well.

The {010} pinacoid is a very peculiar case: two-thirds of water molecules lie in the middle of both slices d^A_{020} and d^B_{020}, while the remaining one-third stay in the outmost layers. In both cases, water dipoles are either oriented parallel to the 010 plane, or their inward components normal to the 010 plane cancel out each other. Moreover, the profile B surely reduces its wavy

https://doi.org/10.1021/acs.jpcc.1c00527
J. Phys. Chem. C 2021, 125, 6923−6932

Table 2. Lattice Coincidences between HH-{010} (Substrate) and Ice$_{I_h}$-{00.1} (Deposit)[a]

host crystal form HH {010}—$P2_1/c$	ranking	lattice vectors (Å)	guest crystal form {00.1}-Ice $_{hex}$	lattice vectors (Å)	difference percent (Δ %)	obliquity (deg)
		[201] = 11.601		[2$\bar{1}$0] = 11.932	+2.85	
		[102] = 11.872		[320] = 11.932	+0.42	
2D-cell area (Å2) and multiplicity	(1a)	112.477 (3×)		123.305 (7×)	+9.62	
		[101] = 6.953		[210] = 7.811	+12.34	
		3×[001] = 19.509		[350] = 19.659	+0.76	
	(1b)	112.477 (3×)		123.305 (7×)	+9.62	
		2×[100] = 12.66		[1$\bar{2}$0] = 11.9323	−6.12	
		[102] = 11.872		[320] = 11.9323	+0.42	
	(2a)	149.536 (4×)		140.920 (8×)	−6.1	
		2×[001] = 13.006		3×[110] = 13.53	+2.78	
		−2×[101] = 13.906		3×[$\bar{1}$00] = 13.53	−4.03	
	(2b)	149.969 (4×)		158.535 (9×)	+5.71	3.39
		2×[101] = 13.906		3×[100] = 13.53	−2.78	
		− 2×[100] = 12.66		3×[010] = 13.53	+6.85	
	(2c)	149.969 (4×)		158.535 (9×)	+5.71	
		3×[001] = 19.509		[250] = 19.726	+1.11	
		2×[100] = 12.663		[2$\bar{1}$0] = 11.932	−6.12	
	(3a)	224.954(6×)		211.380 (12×)	−6.42	1.69
		2×[101] = 13.906		3×[110] = 13.53	−2.78	
		[$\bar{1}$02] = 16.652		[$\bar{1}$30] = 16.261	−2.40	
	(3b)	224.9545 (6×)		211.380 (12×)	−6.42	
		2×[100] = 12.663		[2$\bar{1}$0] = 11.932	−6.12	
		[203] = 18.351		4× [110] = 18.04	−1.72	
	(3c)	224.954(6×)		211.380 (12×)	−6.42	
		2×[101] = 13.906		3×[110] = 13.53	−2.78	
		3×[100] = 18.939		4× [100] = 18.04	−4.98	
	(3d)	224.954(6×)		211.380 (12×)	−6.42	
thickness of the elementary layer (Å)		d_{020} = 5.0588		d_{002} = 3.678	−37.5	
		d_{010} = 10.1176		3×d_{002} = 11.034	+9.05	
		3×d_{020} = 15.1764		4×d_{002} = 14.712	−3.15	

[a]Obliquity represents the angular misfit (°) between the lattice vectors of HH and Ice for each 2D-coincidence cell. The last row indicates the possible coincidences between the thickness of elementary (or multiple) layers of substrate and deposit.

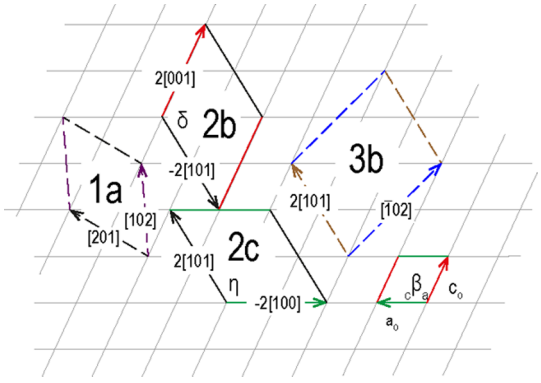

Figure 10. Most representative 2D coincidence cells described in Table 2. In both cases (2b and 2c), that illustrate the pseudo-hexagonality of the Ice/HH epitaxy, the cell vectors are drawn at full stroke; in the other cases, vectors are represented by dashed lines. In the background, the 2D-lattice of $\{010\}_{HH}$ is drawn.

behavior, thanks to the surface relaxation, and hence becomes more similar to profile A. The outcome of this situation is that the difference of the related γ values, with respect to their mean, does not reach 1.7%. Accordingly, the {010} pinacoid should face the surrounding mother phase with two equiprobable profiles.

3.3. Lattice Coincidences between the Pinacoids: {010}-HH and {00.1}-Ice$_{I_h}$.

First of all, here we do recollect that the $\{00.1\}_{I_h}$ form of the hexagonal Ice has a 2D cell which is defined by the symmetry equivalent vectors [100] and [010], having a length of 4.51 Å and related by an angle $\gamma = 120°$. The lattice coincidences between $\{00.1\}_{I_h}$ and $\{010\}_{HH}$ are shown in Table 2.

From Table 2, one can select the 2D supercells that can be proposed in order to obtain the geometrical conditions necessary (but not sufficient) for an epitaxy to occur.

(i) Both supercells with ranking (1a and 1b) have the lowest multiplicity (3× for HH), but their percent area misfit (9.62) is hardly compatible with a good epitaxial relationship.

(ii) Among the supercells having multiplicity 4× for HH, that with ranking (2a) shows a good area misfit but its shape does not comply with any of the cells drawn in Figure 2, where the pseudo-hexagonality of the {010} form is described. Instead, supercells with the ranking (2b and 2c) have the best area misfit, low obliquity, and reproduce exactly two out of the cells drawn in Figure 2. This is a nice surprise; as a matter of fact, the excellent geometrical fit between {00.1}, the most important form of hexagonal polymorph of Ice, and the pseudo-hexagonal {010} form

https://doi.org/10.1021/acs.jpcc.1c00527
J. Phys. Chem. C 2021, 125, 6923−6932

of HH, is a pleasant premise for a good epitaxy to occur between the two crystalline species.

(iii) All the supercells with multiplicity (6×), for HH, show a good area misfit and very good obliquity; nevertheless, none of them satisfy the pseudo-hexagonality of the {010} form, and hence, their epi-conditions are less favorable than those just described in the case (ii).

From the last row in the Table 2, it follows that the percent difference in the thickness of the elementary layers, HH-d_{020} and Ice-d_{002}, is surely incompatible for the absorption of Ice on HH to occur; the same continues to hold for the comparison between HH-d_{010} and Ice-3×d_{002}. Perhaps, during growth, when three HH-d_{020} layers do encounter four Ice-d_{002} layers, the percent difference (3.15) results to be very reasonable for the mixing of the two structures; nevertheless, this event should occur only if the interplay between the Burger's vectors of the two dislocations outcropping the concerned HH and Ice surfaces does fulfill the just mentioned constraint. However, this is very unlikely, and hence, the absorption of Ice into the growing HH should be excluded, at least as far as the form {010} HH is concerned.

Figure 10 represents a synthesis of the just mentioned considerations. Case (1a) is related to the lowest multiplicity (3× referred to HH); both cases (2b and 2c), where the multiplicity is (4×), reproduce the pseudo-hexagonality of the 2D-lattice coincidences, as shown in Figure 2; finally, in case (3b), one out of the four supercells with multiplicity (6×) is drawn. All cases described in Table 2 are drawn in Figure S1 (Supporting Information), not to weigh down the main text.

4. CONCLUSIONS

The observed growth morphology shown in Figure 1, built by the three pinacoids— {100}, {001}, and {10$\bar{1}$}, limited in turn by the dominant {010}, looks sharply different from that calculated, at equilibrium, at 0 K. Two reasons could explain the disappearance of the forms {120} and {011} along with the transition from the quasi-isotropic ES to the {010} flattened GS.

The first one is the adsorption of water molecules, coming from the mother phase, onto the HH surfaces; the reasoning previously put forth about both the position and orientation of water dipoles on the outmost layers of the different HH-d_{hkl} slices suggests that the water adsorption should be "sharply heterogeneous" and thus resulting in the marked differences between the calculated ES (without water adsorption) and the calculated one with an adsorbed monolayer of water.

The second concerns the hypothesis of "ordered water adsorption". This means that water can be adsorbed as an ordered epi-layer of hexagonal {00.1} Ice, as we suggested in the Introduction section, owing to the temperature range in which HH crystallizes. It has been previously shown that the geometrical conditions for the $\{010\}_{HH}//\{00.1\}_{I_h}$ epitaxy are largely fulfilled. Moreover, similar conditions were not found for other HH forms.

Lastly, the growth kinetics of the different HH forms needs to be taken into account. Concerning the $\{010\}_{HH}$ pinacoid, its normal growth rate (R_n) should be ruled by two main factors: (i) the advancement rate (v_∞) of linear steps [100], [101], and [001] limiting the shape of 2D-nuclei and/or spiral arms on the face terraces; and (ii) the adsorption density (ρ_{ads}^{2D}) of 2D-nuclei epi-adsorbed on the terraces in between the advancing steps. Very reasonably, v_∞ and ρ_{ads}^{2D} oppose each other, and hence, R_n of the $\{010\}_{HH}$ pinacoid could be the most affected among the growth rates of the other competing {hkl} growing forms.

To give a quantitative evaluation of our hypotheses, we are working at (a) calculating the interfacial energy values for the best geometrical lattice coincidences described in Table 2, in order to find the probability of epi-heterogeneous nucleation of $\{00.1\}_{I_h}$ on $\{010\}_{HH}$; (b) proposing a theoretical model of normal growth rate of a flat face in which a competition does occur between the advancing steps and the inter-step formation of 2D ordered epi-nuclei of a foreign adsorbed species.

■ ASSOCIATED CONTENT

Supporting Information

The Supporting Information is available free of charge at https://pubs.acs.org/doi/10.1021/acs.jpcc.1c00527.

Absolute atomic coordinates of the four equivalent sets building the unit cell of HH; computational details; and 2D coincidence cells between HH-{010} (substrate) and Ice_{I_h}-{00.1} (deposit) (PDF)

■ AUTHOR INFORMATION

Corresponding Author

Marco Bruno − *Dipartimento di Scienze della Terra, Università degli Studi di Torino, Torino 10125, Italy; SpectraLab s.r.l., Spin-off accademico dell'Università degli Studi di Torino, Torino 10135, Italy;* orcid.org/0000-0002-0161-574X; Email: marco.bruno@unito.it

Authors

Dino Aquilano − *Dipartimento di Scienze della Terra, Università degli Studi di Torino, Torino 10125, Italy;* orcid.org/0000-0002-3908-928X

Linda Pastero − *Dipartimento di Scienze della Terra, Università degli Studi di Torino, Torino 10125, Italy; SpectraLab s.r.l., Spin-off accademico dell'Università degli Studi di Torino, Torino 10135, Italy;* orcid.org/0000-0002-9453-9503

Stefano Ghignone − *Dipartimento di Scienze della Terra, Università degli Studi di Torino, Torino 10125, Italy*

Complete contact information is available at: https://pubs.acs.org/10.1021/acs.jpcc.1c00527

Notes

The authors declare no competing financial interest.

■ ACKNOWLEDGMENTS

The present study has been partly funded by the project PRIN 2017 (2017L83S77), of the Italian Ministry for Education, University and Research (MIUR).

■ REFERENCES

(1) Bär, G.; Barthel, D.; Baumann, N.; Behrendt, W.; Berg, L.; Best, E.; Bonn, K. D.; Born-Heck, P.; Chavizon, V. A.; Cloos, E.; et al. *Gmelin Handbook of Inorganic Chemistry*; Springer: Berlin, Heidelberg, 1973.

(2) Mitscherlich, E. Über der Wasserfreie und Wasserhaltige Chlornatrium, Jodnatrium und Bromnatrium. *Ann. Phys.* **1829**, *93*, 385−388.

(3) Craig, J. R.; Fortner, R. D.; Weand, B. L. Halite and hydrohalite from Lake Bonney, Taylor Valley, Antarctica. *Geology* **1974**, *2*, 389−390.

(4) Craig, J. R.; Light, J. F.; Parker, B. C.; Mudrey, M. G., Jr. Identification of hydrohalite. *Antarct. J.* **1975**, *10*, 178−179.

(5) Swenne, D. A. The eutectic crystallization of NaCl·2H_2O and Ice. Ph.D. Thesis, Technische Hogeschool, Eindhoven, 1983.
(6) Daniel, I.; Caracas, R. Hydrohalite: properties of a major hydrate in the H_2O-NaCl binary. *AGU Fall Meeting Abstracts*, 2009.
(7) Wise, M. E.; Baustian, K. J.; Koop, T.; Freedman, M. A.; Jensen, E. J.; Tolbert, M. A. Depositional ice nucleation onto crystalline hydrated NaCl particles: a new mechanism for ice formation in the troposphere. *Atmos. Chem. Phys.* **2012**, *12*, 1121−1134.
(8) Wagner, R.; Möhler, O. Heterogeneous ice nucleation ability of crystalline sodium chloride dehydrate particles. *J. Geophys. Res.: Atmos.* **2013**, *118*, 4610−4622.
(9) Thürmer, K.; Bartelt, N. C. Growth of multilayer ice films and the formation of cubic ice imaged with STM. *Phys. Rev. B: Condens. Matter Mater. Phys.* **2008**, *77*, 195425−195435.
(10) Maier, S.; Lechner, B. A. J.; Somorjai, G. A.; Salmeron, M. Growth and Structure of the First Layers of Ice on Ru(0001) and Pt(111). *J. Am. Chem. Soc.* **2016**, *138*, 3145−3151.
(11) Hartman, P.; Perdok, W. G. On the Relations Between Structure and Morphology of Crystals. I. *Acta Crystallogr.* **1955**, *8*, 49−52.
(12) Hartman, P.; Perdok, W. G. On the Relations Between Structure and Morphology of Crystals. II. *Acta Crystallogr.* **1955**, *8*, 521−524.
(13) Hartman, P.; Perdok, W. G. On the Relations Between Structure and Morphology of Crystals. III. *Acta Crystallogr.* **1955**, *8*, 525−529.
(14) Crawford, M. L. Phase equilibria in aqueous fluid inclusions. In *Fluid Inclusions: Applications to Petrology*; Hollister, L. S., Crawford, M. L., Eds.; Mineralogical Association of Canada Short Course Handbook: Quebec, 1981; pp 75−100.
(15) Klewe, B.; Pedersen, B. The crystal structure of Sodium Chloride Di-hydrate. *Acta Crystallogr., Sect. B: Struct. Crystallogr. Cryst. Chem.* **1974**, *30*, 2363−2371.
(16) Palache, C.; Berman, H.; Frondel, C. *Dana System of Mineralogy*, 7th ed.; John Wiley & Sons: New York, 1951.
(17) Anthony, J. W.; Bideaux, R. A.; Bladh, K. W.; Nichols, M. C. *Handbook of Mineralogy*; Mineral Data Publishing: Tucson, Arizona, 1997; Vol. III Halides, Hydroxides, Oxides, p 628.
(18) Dovesi, R.; Civalleri, B.; Orlando, R.; Roetti, C.; Saunders, V. R. Ab initio quantum simulation in solid state chemistry. In *Reviews in Computational Chemistry*; Lipkowitz, B. K., Larter, R., Cundari, T. R., Eds.; John Wiley & Sons, Inc.: New York, 2005; pp 1−125.
(19) Dovesi, R.; Orlando, R.; Civalleri, B.; Roetti, C.; Saunders, V. R.; Zicovich-Wilson, C. M. CRYSTAL: a computational tool for the ab initio study of the electronic properties of crystals. *Z. Kristallogr.* **2005**, *220*, 571−573.
(20) Dovesi, R.; Saunders, V. R.; Roetti, C.; Orlando, R. C.; Zicovich-Wilson, M.; Pascale, F.; Civalleri, B.; Doll, K.; Harrison, N. M.; Bush, I. J.; et al., *CRYSTAL14 User's Manual*, University of Torino: Torino, 2014.
(21) Pisani, C.; Dovesi, R.; Roetti, C. Hartree-Fock ab-initio treatment of crystalline systems. *Lecture Notes in Chemistry*; Springer: Berlin, Heidelberg, New York, 1988.
(22) Becke, A. D. Density-functional thermochemistry. III. The role of exact exchange. *J. Chem. Phys.* **1993**, *98*, 5648−5652.
(23) Lee, C.; Yang, W.; Parr, R. G. Development of the Colle-Salvetti correlation-energy formula into a functional of the electron density. *Phys. Rev. B: Condens. Matter Mater. Phys.* **1988**, *37*, 785−789.
(24) Stephens, P. J.; Devlin, F. J.; Chabalowski, C. F.; Frisch, M. J. Ab Initio calculation of vibrational absorption and circular dichroism spectra using density functional force fields. *J. Phys. Chem.* **1994**, *98*, 11623−11627.
(25) Toschev, S. Homogeneous nucleation. In *Crystal Growth. An Introduction*; Hartman, P., Ed.; Elsevier, North Holland: Amsterdam, 1973; pp 1−49.

https://doi.org/10.1021/acs.jpcc.1c00527
J. Phys. Chem. C 2021, 125, 6923−6932